

RESEARCH PAPER

NUMERICAL AND EXPERIMENTAL STUDY OF CERAMIC/STEEL COMPOSITE FOR STRUCTURAL APPLICATIONS

Olawale Monsur Sanusi^{1,2*}, Olatunde Ajani Oyelaran², Mounir Methia^{1,3}, Anurag Dubey¹, Adeolu Adesoji Adediran⁴

¹INSA CVL, Univ. Tours, Univ. Orléans, LaMé, 3 rue de la Chocolaterie, BP 3410, 41034 Blois Cedex, France

²Department of Mechanical Engineering, Federal University Oye-Ekiti, Ekiti State, Nigeria

³Laboratoire de Mécanique, Matériaux et Energétique (L2ME), Faculté de Technologie, Université de Bejaia, 06000 Bejaia, Algeria

⁴Department of Mechanical Engineering, Landmark University, Omu Aran, Kwara State, Nigeria

*Corresponding author: olawalem.sanusi@fuoye.edu.ng, tel.: +33602120550, LaMé / INSA Centre Val de Loire, 41000, Blois, France

Received: 06.01.2021

Accepted: 11.03.2021

ABSTRACT

The terminal ballistics is the study of science that deals with the interaction involved in two impacting bodies. Identifying the optimum thickness ratio of layered composites that offers efficient resist to impending projectile is a great challenge in ballistics engineering. This research focused on the high-impact resistance of layered composite comprising of alumina ceramic and armour steel using numerical approach (Abaqus) in determining the composite thickness ratio. The composite was designed to have ceramic as the facial plate with armour steel as its backing plate. From the numerical study, the ceramic thickness was varied (6, 8, 10, 12 mm) while keeping the thickness of backing steel constant (7 mm). The projectile, 7.62 mm armour-piercing (AP), was set with a velocity of 838 m/s and made to impact the different ceramic-steel composite target configurations at zero obliquity. The study captured fracture processes of the ceramic, the deformation of projectile, and backing steel. An effective optimum thickness ratio of 1.4 (ceramic:steel; 10/7) for the ceramic/steel components with less deformation of the backing steel was found. Thereafter, the result of the numerical study was validated by experimental ballistic investigation of the determined optimum ceramic/steel ratio. The experiment corroborated the simulation results as the alumina ceramic provided efficient protection to armour steel component after a severe interaction with the impacting projectile.

Keywords: ceramics; steel; composites; armour; terminal ballistics

INTRODUCTION

Armour structure provides ballistic defeat to imminent projectiles or blast fragments. Traditionally, ballistic protection is primarily made of high hardness steel owing to its high strength and rigidity. However, most systems requiring ballistic protection are mobile (military vehicle, tank, aircraft and/or military/security personnel). Thus, thickness of the protective materials, related to weight, becomes a critical issue in armour design. Two, it is becoming easy to defeat strong steel via armour piecing (AP) projectile that causes a major setback for conventional steel. Understanding this weakness, ammunition designers are replacing standard metallic projectile nose with toughened-ceramic nose in an attempt to increase projectile penetration capability in protection targets [1]. These led to search for high-performance but lightweight and low-cost protective materials (for personnel and vehicles) to improve manoeuvrability, survivability and reduce injury when subject to threats including blast [2,3]. Thus, enhanced mobility, high strength to weight ratio with the high impact resistance are the primary concept of lightweight armour design [4]. Consequently, ceramic-steel composites have been introduced to offer the solution for efficient lightweight armours [5-10]. Precisely, low density, high hardness, high rigidity and compression strength of ceramics [1,5] makes it popular and

suitable for armour systems; including aircraft structures, personal armour and military vehicles [11-15]. Several ceramic materials are used for facial ballistic armours: alumina [16-18], boron carbide (B4C) [19], silicon carbide (SiC) [20]. The backing steel provides structural integrity as ceramics lack strength under tension [21].

The experimental research requires many samples to be prepared and evaluated ballistically against several projectiles at varying conditions. This consumes much time, cost and often lead to abandoning of quite a few scenarios. So, to predict various cases of material behaviour, modelling and simulation are adopted through discrete numerical methods (e.g. finite element method, FEM or smoothed particle hydrodynamics, SPH) [22]. Besides, the high speed involved in terminal ballistics makes it challenging to visualize and analyze projectile-target interaction damage, but numerical simulation permits such studies [23].

Fawaz et al. [24] used finite element code LS-DYNA in simulating the normal and oblique ballistic impact of projectile against alumina ceramic plate and carbon/epoxy composite at low velocity (315 m/s). They found that the bullet erosion in the oblique impact was slightly more than that of normal impact, while the distributions of global kinetic, internal and total energy versus time were similar for normal and oblique impacts. Akella [7] studied the layering effect of ceramic

armour in an effort to improving toughness property over aluminium-alloy backing using numerical methods of Autodyn. A monolithic ceramic or layers of ceramic at a given thickness were studied over a constant thickness of the backing. The simulated impact velocity was 800 m/s using 5 mm diameter steel projectile. It was observed that increasing the layers lowered the penetration resistance of ceramic but with better multi-hit capacity when compared with monolithic ceramic of the same strength. It was reported that the reduction in layer thickness leads to increase in the system strength. Alumina ceramic had been previously prepared by sintering process from purified corundum [25, 26]. This study strives to determine the ballistic influence of the ceramic on ceramic/steel composite as well as finding the optimum thickness of the ceramic required to make an applied component of ceramic/steel armour system for structural ballistic applications.

2. MODEL AND MATERIAL DESCRIPTION

The simulations models were developed and carried out using the Abaqus/Explicit 6.12 simulation software in a computer equipped with Intel core i5 CPU at 2.20 GHz [27].

2.1 Creation of the models

2.1.1 Projectile

The conical-point cylindrical projectile was modelled as 7.62 mm in diameter using the revolving tool after creating the 2D profile with a length of 28.1 mm; following NIJ Standard 0108.01 (1985) [28]. The revolve command was set at 90° to produce a quarter model of the projectile (symmetry) as shown in Fig. 1(a).

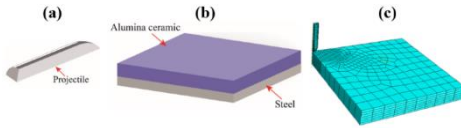


Fig. 1 Model and finite element representation of impacted alumina ceramic/steel composite armour target (a) projectile (b) laminate (c) projectile-laminate finite element assembly.

2.1.2 Components (layers) of the armour system

The rectangular armour target has its frontal plate as alumina ceramic with varying thickness (6, 8, 10 and 12 mm), and a 7 mm steel backing. These plates were created by extrusion tool of ABAQUS after creating 2-D square profiles (50 X 50 mm), Fig. 1b. Then the parts created separately were imported into assembly environment of the software. Mates command were applied to the components to create the parts assembly. The assembled meshed model in the ABAQUS interface is as shown in Fig. 1c.

2.2 Models definition and constraints

Two different material models were used for this simulation. The Johnson-Cook (JC) constitutive model was used to predict the material behaviour of the backing steel plate and projectile. JC model is commonly used to predict the material response of metals: armour steel, aluminium alloy and projectile material [28]. The model is supported by most finite element code, and the model constitutive dynamic flow stress (σ_f) relation is expressed in Eq. (1) [29-32].

$$\sigma_f = \left\{ A + B(\dot{\epsilon}_o^p)^N \right\} \left[1 + C \ln \frac{\dot{\epsilon}_o^p}{\dot{\epsilon}_o} \right] \left[1 - \left(\frac{T - T_o}{T_m - T_o} \right)^M \right] \quad (1.)$$

Where, $\dot{\epsilon}_o$ is the equivalent plastic strain rate, $\dot{\epsilon}_o^p$ is the effective plastic strain rate, $\dot{\epsilon}_o^p$ is the effective plastic strain. T_o and T_m are reference and melting temperature, respectively. A, B, C, N, M are the material property constants required for the material model.

The JC model is also incorporated with a failure model which is related to von Mises stress ($\bar{\sigma}$), the three normal stresses average (σ^m), temperature, T and $\dot{\epsilon}_o^p$. The expressions for the damage, D is given in Equation 2 - 3, according to Lamberts [32].

$$D = \left[\frac{\dot{\epsilon}_o^p}{\dot{\epsilon}_o} \right] \quad (2.)$$

$$\dot{\epsilon}_o = \left\{ D_1 + D_2 \exp \left(D_3 \frac{\sigma^m}{\bar{\sigma}} \right) \right\} \left[1 + D_4 \ln \frac{\dot{\epsilon}_o^p}{\dot{\epsilon}_o} \right] \left[1 + D_5 \frac{T - T_o}{T_m - T_o} \right] \quad (3.)$$

Where D_1, D_2, D_3, D_4 and D_5 are material parameters. Johnson Holmquist (JH-2) material models was implemented into ABAQUS as user-defined material model in predicting the material behaviour of the alumina. JH-2 predicts mechanical characteristics of brittle materials (e.g. rock, ceramics, concrete) subjected to excessive loading [29]. The key features of the model comprise pressure-dependent strength, damage and fracture, substantial strength after fracture, bulking and strain rate effects [33, 34]. According to Kędzierski et al. and Ming and Pantalé [29, 35], the normalized equivalent stress, σ^* , is given in Eq (4),

$$\sigma^* = \sigma_i^* - D(\sigma_i^* - \sigma_f^*) \quad (4.)$$

Where, σ_i^* is the normalized intact equivalent stress; σ_f^* is the normalized fracture strength stress and D is the damage variable; ($0 \leq D \leq 1$). Eqs (5) and (6) give the expressions for the normalized intact equivalent stress and normalized fracture equivalent stress, respectively given as

$$\sigma_i^* = A(P^* + T^*)^N (1 + C \ln(\dot{\epsilon}^*)) \quad (5.)$$

$$\sigma_f^* = B(P^*)^M (1 + C \ln(\dot{\epsilon}^*)) \quad (6.)$$

A, B, C, M and N are material constants; P^* is the normalized pressure; $\dot{\epsilon}^*$ is the normalized strain-rate; with energy conversion factor (β) and equation of state parameters (K_1, K_2, K_3).

The material property constants required for the models were sourced from literature [7, 24, 29, 33, 34] and presented in Tables 1 and 2. The constrained tied with Surface-To-Surface Contact element was selected to connect the ceramic and backing plate. The boundary or contact procedures between the projectile and the armour system were defined with Contact-Erasing-Surface-To-Surface. The nodes that make up the projectiles mesh were allocated an initial velocity of 838m/s in accordance to (NIJ Standard 0108.01, 1985). The projectile was impacted normally on to the different ceramic-steel composite target configurations.

3. NUMERICAL SIMULATION RESULTS

3.1 Projectile/target interaction

For this simulation, the evaluating parameter was the optimum thickness of the ceramic on armour system in order to avoid any complete penetration of the target at the limit velocity of the projectile, as well as saving both space and weight for a

lightweight armour system. Therefore, various target configurations are modelled and simulated by varying the ceramic thickness (6, 8, 10, 12 mm) over a constant 7 mm backing armour steel.

Table 1 JC model parameters for projectile core and armour steel

Property	Unit	Projec-tile	Backing steel
Density	g/cm ³	7.85	7.85
Young's modulus	GPa	202	202
Poisson ratio		0.3	0.3
JC Constants:			
A	GPa	1,576	0,849
B	GPa	2,906	1,39
N		0,1172	0,0923
C		0,00541	0,00541
M		0,87	0,87
Melting temperature	K	1800	1800
Transition temperature	K	293	293
Referential strain rate	1/s	1	1
Failure Constants:			
D ₁		0,0356	-0,4
D ₂		0,0826	1,5
D ₃		-2,5	-0,5
D ₄		0	0,002
D ₅		0	0,61

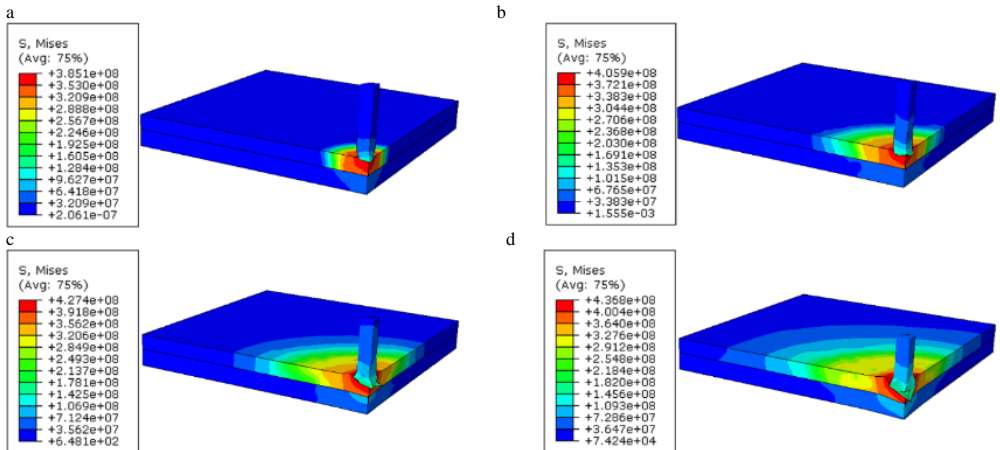
Table 2 JH-2 model parameters for alumina ceramic

Property	Unit	Alumina Ceramic
Density	kg/m ³	3700
Shear modulus	GPa	90,16
JH-2 Constants:		
A		0,93
B		0,31

N		0,6
C		0
M		0,6
Referential strain rate	1/s	1
JH-2 Failure:		
D ₁		0,005
D ₂		1
EOS Constants:		
K ₁	Pa	1,3095 E11
K ₂	Pa	0
K ₃	Pa	0
Beta, β		1

3.1.1 6mm-ceramic/7mm-backing steel (6-7 Armour System)

The computational impact process for the 6-7 armour system at different time interval is shown in Fig. 2(a-f). It illustrates the position of the projectile in the impact process at different times, according to the von Mises stress. By the impact of the projectile, fractures are initiated instantaneously in the facial ceramic plate around the region of projectile impact periphery. The fractures occur in 2 μs of the total 40 μs of projectile-armour target interaction which is ascribed to the extreme compressive stress at that point. The ceramic plate is observed to be fully eroded by the projectile in Fig. 2(f-h); all depict the same final stage of erosion. Fig. 2(g) only carries the meshing feature, while the worn projectile was hidden (removed) in Fig. 2(h), from the impact site, in order to vividly reveal the destruction state at 40 μs. A conical crushed ceramic region remains in front of the deformed projectile while the fractures reach the interface of ceramic-metal composite. The result is in agreement with the literature [24]. At the interface, the projectile is seen to be squashed, stopped but caused severe bulging on the armour steel backing.



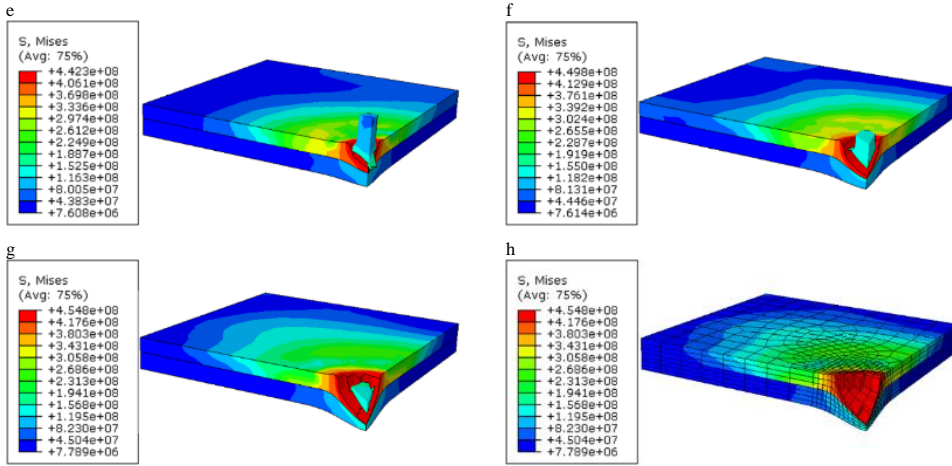
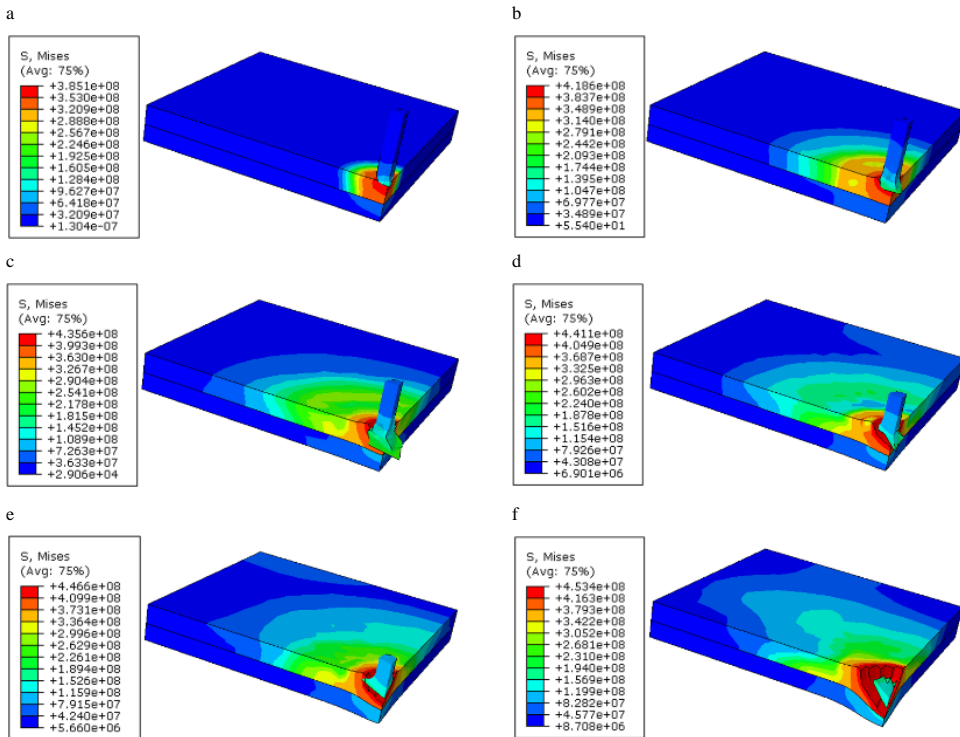


Fig. 2 Impact processes for 6mm ceramics/7mm backing steel composite

3.1.2 8 mm-ceramics/7mm-backing steel (8-7 Armour System)

A similar occurrence is observed when the configuration with 8mm-ceramics/7mm-backing steel plate was impacted with the

same projectile; see Fig. 3. The gradual erosion of the projectile and the ceramic commenced from Fig. 3(a-f), while tensile deformation of the backing plate without complete perforation was also observed but is less than 6-7 armour system.



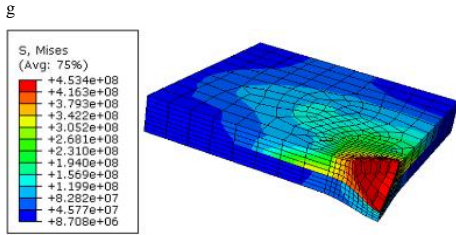


Fig. 3 Impact processes for 8mm ceramics/7mm backing steel composite

3.1.3 10 mm-ceramics/7mm-backing steel (10-7 Armour System)

The gradual erosion of the projectile and the ceramic commenced from Fig. 4(a) through to Fig. 4(g), while tensile deformation of the backing plate without perforation was observed. The worn projectile was hidden (Fig. 4(f and g)) from the impact site in order to reveal the destruction level.

Interestingly, 10-7 armour system, in comparison with 6-7 and 8-7 armour systems (Table 3 and Fig. 6), is observed to leave less deformation or stress on the backing after the projectile-ceramic mass erosion. Residue thickness of the compressed fractured ceramic layer is also visible after the impact phenomenon; Fig. 4(e and g).

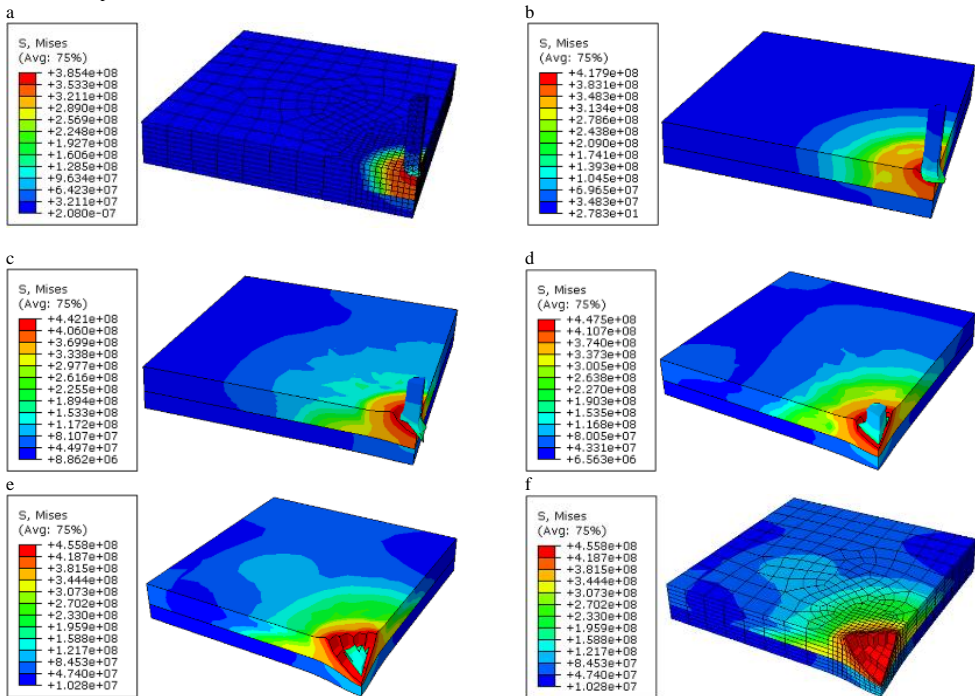


Fig. 4 Impact processes for 10mm ceramics/7mm backing steel composite

3.1.4 12 mm-ceramics/7mm-backing steel (12-7 Armour System)

Similarly, on increasing the ceramic thickness to 12 mm over the same thickness of metal backing, the projectile penetration phenomenon was the same with low bulging of the backing steel, Fig. 5. The erosion of the projectile and ceramic commenced from Fig. 5(a-f). The worn projectile was hidden (removed), in Fig. 5(f). The 12-7 configuration, in comparison with 10-7 armour systems (Table 3), is also observed to leave

less deformation or tensile stress on the backing after the projectile-ceramic mass erosion. In comparing with 10-7 system, higher residue thickness of the fractured ceramic layer is visible after the impact phenomenon, Fig. 5(f).

At various stages, Fig. 2 - 5 have revealed the resulting contours of damage during the impact processes. The damages were initiated at the instance of affecting points, followed with the fracture front growing outwards, generally, in the radial direction. It was also appreciated that the impact generated compression on the armour laminate systems and this travelled (across the laminates) considerably faster than the damage

fronts. Usually, at the second stage of the penetration phase of the projectile, the compression waves were always observed to have travelled through the thickness of the ceramic and the metal composite. The metallic backing experienced lesser compression as it is seen from the simulation result that the backing has the next deep blue colouration to the original deep blue colour of the backing plate. As reported by Cronin et al. [36] that used LS-DYNA tool for simulating impact on ceramic material, the wave was reflected at the free surface bringing about a tensile wave with sufficient pressure to initiate tensile

or spall failure of the ceramic component. The penetration of the projectile through the target materials led to erosion and massive change of the projectile shape. In addition, the deformed bullet left crater of higher diameter than the projectile, which is in agreement with the works of Hub and Kneys [37] and Şenyilmaz et al. [23]. The deformation on the backing steel, as the ceramic get thicker, was observed to reduce, probably due to energy released from the fractured ceramic particles [38].

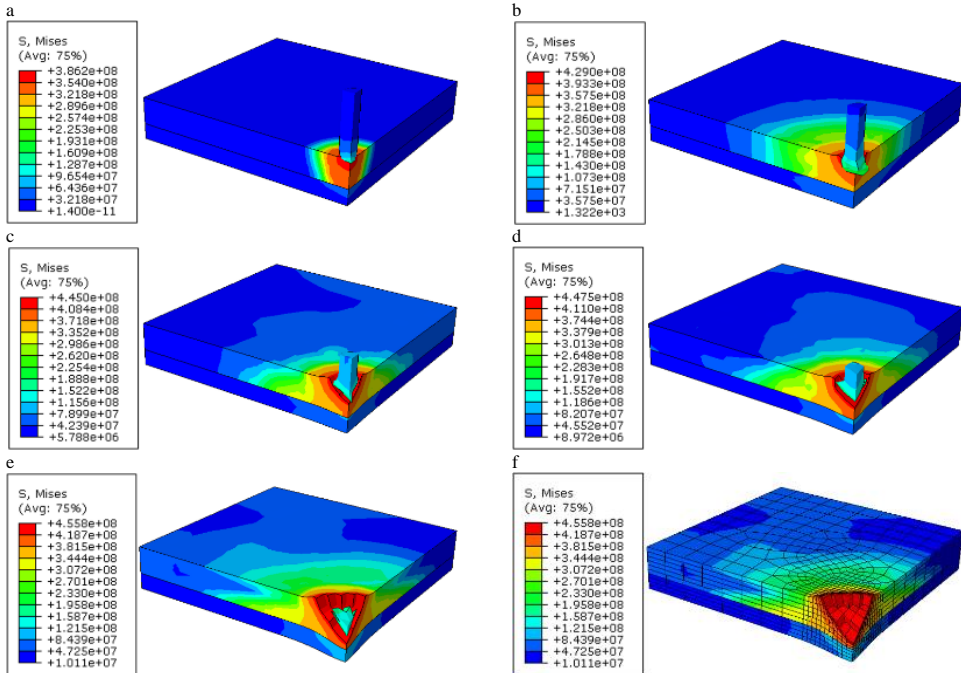


Fig. 5 Impact processes for 12mm ceramics/7mm backing steel composite

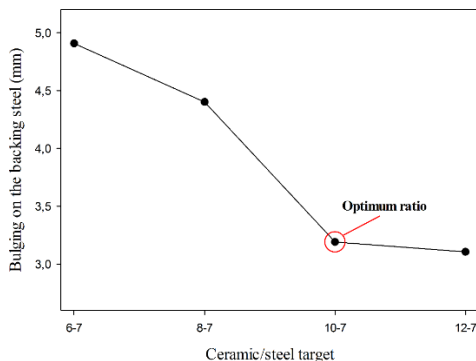


Fig. 6 Bulging left on the backing armour steel after the fracture of the facial ceramic on the different ceramic/steel composite configurations

Table 3 shows the final stages of the different simulated configurations in order to compare the deformation levels. Fig. 6 depicts that the level of bulging left on the backing steel reduced with increase in ceramic thickness until an optimal

ceramic thickness 10 mm is attained. Beyond this thickness (ceramic:steel = 10:7), increase in the ceramic thickness insignificantly influenced the ballistic resistance of the target system against 7.62 mm AP projectile. Therefore, the 10/7 armour assembly was considered to be the optimum system which could save space and weight in the composite armour assembly. Hence, the composite was selected and processed for experimental validation in section 4. From the numerical simulation result, it is concluded that the optimum erosion of 7.62 mm projectile could be achieved with a composite armour system comprising of 10 mm thick alumina ceramic on the steel plate.

3.2 Deformation energy history

The global energy history plots generated during the impact process for 10⁻⁷ armour system is presented in Fig. 7. It was observed that the kinetic energy (Fig. 7a) gradually reduced as the projectile penetrated the armour. In contrast, the system internal energy was observed to have increased, which agrees with literature [24, 39]. The dissipation of kinetic energy from 1.4 x 10³ KJ to approximately zero in 40 µs resulted from deceleration on the velocity of the projectile, mass erosion of both the projectile and the armour system and the heat

losses associated with the impact phenomenon. The projectile kinetic energy is transferred to the armour composite system after impact. Hence, the internal energy, at a lower rate, increased from zero to its peak of about 900 kJ at 40 μ s, Fig. 7b. The difference in the energy rate caused the total energy of the system to increase with decrease in kinetic energy, Fig. 7c. KE is computed by summation of $0.5 (\text{nodal mass} \times \text{nodal velocity}^2)$ for both the nodes of projectile and the target. When this node-velocity comes to zero, the projectile comes to a complete rest.

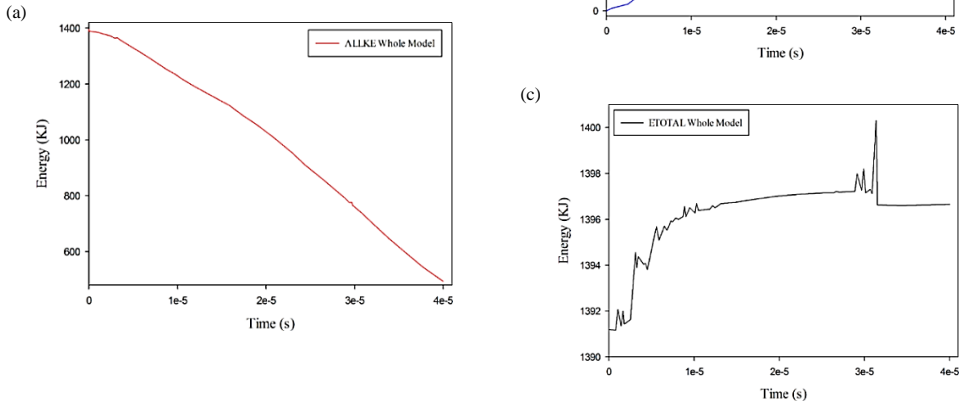


Fig. 7 Computed global energy (kJ) against time (μ s) (a) kinetic energy (b) internal energy (c) total energy

Table 3 Comparison of last stages of impact simulation in armour assembly configurations

Armour configuration	Free edge laminate with projectile	Meshed laminate without projectile
6-7		
8-7		
10-7		
12-7		

4. EXPERIMENTAL BALLISTIC STUDY

Normally, the ability of armour to stop bullets, ballistics effectiveness, is not determined by visual inspection but must be inferred from the results of live-firing test [40]. Sintered alumina ceramic ($10 \times 120 \times 120$ mm) prepared by sintering process [26] was used as the facial plate; and **Table 4** gives the physical properties of the sintered alumina (AC-86.6). The ceramic was laminated onto $7 \times 120 \times 120$ mm armour steel (donated by Defence Industries Corporation of Nigeria), **Fig. 8a**, using synthetic Araldite[®] epoxy adhesive and then left to dry for 24 hr under 26 MPa. Thereafter, the glued plates were wrapped with transparent polypropylene to enhance the firmness, **Fig. 8b**. The prepared samples were first conditioned at 23 °C for 24 h [27,41,42]. Test was taken at normal obliquity, 15 m from the weapon muzzle with projectile velocity maintained at 838 ± 15 m/s. Light automatic rifle was used for firing 7.62×51 armour piercing projectile (AP).

Table 4 Mechanical properties of sintered ceramic

	ρ g/cm ³	CS MPa	FS MPa	E GPa	K _{1c} MPa.m ^{1/2}	BHN
AC-86.6	3.45	1912	295	270	3.75	75

Note: CS-compressive strength, FS-flexural strength, E-Young's modulus, K_{1c}-Fracture toughness and BHN-hardness

4.1 Evaluating armour steel

The as-received armour steel was first solely hit with 7.62×51 mm AP. The result of the impact against the armour steel plate at 0° obliquity is depicted in **Fig. 9**. The plate was penetrated completely through rearward petalling mode of perforation failure. This was expected as the strongest steel could easily be defeated by AP projectile [3]. The plate slightly bent inward at the impact of the projectile, which induced high circumferential stress at the impact point, and the compressive wave propagated inward leading to the failure of the armour steel [43]. The reverse side of the armour plate showed minute ductile-hole enlargement deformation, which is comparable to literature [44]. This failure mode is typically observed in a high ductile metal in which the nose of the conical bullet concentrates stresses at the contact point and results in intense deformation of the crater axis [45, 46].

4.2 Composite: Laminate of alumina ceramic and armour steel

Fig. 10(a) depicts laminate of ceramic and armour steel after impact process. The compression at the point of impact caused the debonding of ceramic and failed by pulverization into several pieces, while the backing armour steel was intact after the projectile impact. The pulverization of the ceramic occurred after the formation of microcracks, which developed into comminuted zone, also referred to as Mescall zone [9]. The ceramic, supported by high strength armour steel, significantly interacted with the projectile and lowered its energy, which resulted in the protection of armour steel with less bulge on it, **Fig. 10(b)**. As similarly observed by Guo et al. [8], bi-layered structure of ceramic/metal showed better ballistic performance because the ceramic eroded the bullet through cracking while the metal absorbed the remnant projectile kinetic energy by its deformation. Thus, the experimental results agree with the numerical simulation that predicted the wearing of the projectile by the ceramic, while the backing steel was ultimately protected.

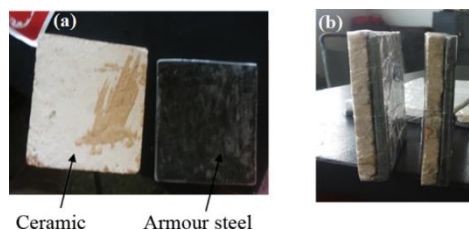


Fig. 8 (a) Sintered ceramic (left) and backing steel (right); (b) assembled composite

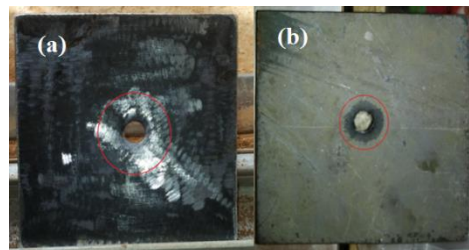


Fig. 9 Armour steel penetrated by 7.62 AP projectile (a) Front view (b) back view

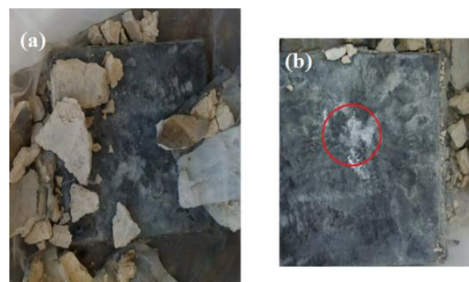


Fig. 10 (a) Fractured ceramic (b) Impression of the bullet impact on armour backing plate (red circle) after impact test

5. CONCLUSION

The numerical investigation of alumina ceramic/steel armour composite impacted by 7.62 mm AP projectile was studied to determine the optimal ceramic thickness required for providing high ballistic protection. The study captured the deformation of projectile, backing steel and fracture processes of the ceramic. The projectile was set with an initial velocity of 838m/s as per NIJ Standard and impacted on different ceramic–steel composite target configurations at zero obliquity. An optimum thickness ratio of 10:7 (ceramic/steel ratio) was found to offer the most effective composite armour system with the least trauma on the target steel. The simulation results depicted severe interaction of the projectile and the composite, wherein gradual erosion and retardation of the projectile by the ceramic component was achieved leaving armour steel plate protected. Finally, the experimental result corroborated the simulation result as the alumina ceramic provided efficient protection to armour steel component despite its failure. Therefore, the result of the finite element model was found useful in the improvement of lightweight armour laminate system design.

ACKNOWLEDGEMENT

The Defence Industries Corporation of Nigeria (DICON) is acknowledged for providing the armour steel plate and facilities for the ballistic experimental evaluation of the composites.

REFERENCES

1. D. Hu, J. Wang, L. Yin, Z. Chen, R. Yi, C. Lu: Experimental study on the penetration effect of ceramics composite projectile on ceramic/A3 steel compound targets, *Def. Technol.*, 13, 2017, 281–287. <https://doi.org/10.1016/j.dt.2017.05.011>.
2. B. Quéfélec, M. Dartois: Ceramic-faced molded armor, in: *Lightweight Ballistic Composites*, Second ed., A. Bhatnagar (Ed.), Amsterdam: Woodhead Publishing, Elsevier Ltd., 2016, p. 369–391. <https://doi.org/10.1016/B978-0-08-100406-7.00013-1>.
3. J.R. Denzel: *Determination of shock properties of ceramic corbit 98: 98% alumina*, MSc Thesis Naval Postgraduate School (2010). <https://apps.dtic.mil/dtic/tr/fulltext/u2/a524549.pdf>.
4. V.C. Khan, A.K. Veldanda, G. Balaganesan, M.S. Sivakumar: Numerical study on multi layered target material subjected to impact loading, *Lat. Am. J. Solids Struct.*, 15, 2018, 1–18. <https://doi.org/10.1590/1679-78254156>.
5. R. Yi, L. Yin, J. Wang, Z. Chen, D. Hu: Study on the performance of ceramic composite projectile penetrating into ceramic composite target, *Def. Technol.*, 13, 2017, 295–299. <https://doi.org/10.1016/j.dt.2017.05.009>.
6. E. Medvedovski: Ballistic performance of armour ceramics: Influence of design and structure Part 2, *Ceram. Int.*, 36, 2010, 2117–2127. <https://doi.org/10.1016/j.ceramint.2010.05.022>.
7. K. Akella: Studies for Improved Damage Tolerance of Ceramics Against Ballistic Impact Using Layers, *Procedia Eng.*, 173, 2017, 244–250. <https://doi.org/10.1016/j.proeng.2016.12.006>.
8. X. Guo, X. Sun, X. Tian, G.J. Weng, Q.D. Ouyang, L.L. Zhu: Simulation of ballistic performance of a two-layered structure of nanostructured metal and ceramic, *Compos. Struct.*, 157, 2016, 163–173. <https://doi.org/10.1016/j.compstruct.2016.08.025>.
9. L. Jinzhu, Z. Liansheng, H. Fenglei: Experiments and simulations of tungsten alloy rods penetrating into alumina ceramic/603 armor steel composite targets, *Int. J. Impact Eng.*, 101, 2017, 1–8. <https://doi.org/10.1016/j.ijimpeng.2016.09.009>.
10. J.D. Clayton: Modeling and Simulation of Ballistic Penetration of Ceramic-Polymer-Metal Layered Systems, *Math. Probl. Eng.*, 2015, 709498. <https://doi.org/10.1155/2015/709498>.
11. B. Tepeduzu, R. Karakuzum: Ballistic performance of ceramic/composite structures, *Ceram. Int.*, 45, 2019, 1651–1660. <https://doi.org/10.1016/j.ceramint.2018.10.042>.
12. R. Chi, A. Serjoui, I. Sridhar, T.E.B. Geoffrey: Pre-stress effect on confined ceramic armor ballistic performance, *Int. J. Impact Eng.*, 84, 2015, 159–170. <https://doi.org/10.1016/j.ijimpeng.2015.05.011>.
13. Q. Wang, Z. Chen, Z. Chen: Design and characteristics of hybrid composite armor subjected to projectile impact, *Mater. Des.*, 46, 2013, 634–639. <https://doi.org/10.1016/j.matdes.2012.10.052>.
14. M.V. Silva, D. Stainer, H.A. Al-Qureshi, O.R.K. Montedo, D. Hotza: Alumina-Based Ceramics for Armor Application: Mechanical Characterization and Ballistic Testing, *J. Ceram.*, 2014, 2014, 1–6. <https://doi.org/10.1155/2014/618154>.
15. D. Luo, Y. Wang, F. Wang, H. Cheng, Y. Zhu: Ballistic behavior of oblique ceramic composite structure against long-rod tungsten projectiles, *Materials*, 12, 2019, 1–13. <https://doi.org/10.3390/ma12182946>.
16. J. Venkatesan, M.A. Iqbal, V. Madhu: Ballistic Performance of Bilayer Alumina/Aluminium and Silicon Carbide/Aluminium Armours, *Procedia Eng.*, 173, 2017, 671–678. <https://doi.org/10.1016/j.proeng.2016.12.141>.
17. A.Y. Badmos, D.G. Ivey: Characterization of structural alumina ceramics used in ballistic armour and wear applications, *J. Mater. Sci.*, 36, 2001, 4995–5005. <https://doi.org/10.1023/A:1011885631876>.
18. E.G. Pickering, M.R. O’Masta, H.N.G. Wadley, V.S. Deshpande: Effect of confinement on the static and dynamic indentation response of model ceramic and cermet materials, *Int. J. Impact Eng.*, 110, 2017, 123–137. <https://doi.org/10.1016/j.ijimpeng.2016.12.007>.
19. S.G. Savio, K. Ramanjaneyulu, V. Madhu, T.B. Bhat: An experimental study on ballistic performance of boron carbide tiles, *Int. J. Impact Eng.*, 38, 2011, 535–541. <https://doi.org/10.1016/j.ijimpeng.2011.01.006>.
20. M. Cegła, W. Habaj, W. Stepniak, P. Podgorzak: Hybrid Ceramic-Textile Composite Armour Structures for a Strengthened Bullet-Proof Vest, *Fibres Text. East. Eur.*, 1, 2015, 85–88. <https://doi.org/www.fibtex.lodz.pl/2015/1/85.pdf>.
21. C. Evci, M. Gülgeç: Effective damage mechanisms and performance evaluation of ceramic composite armors subjected to impact loading, *J. Compos. Mater.*, 48, 2014, 3215–3236. <https://doi.org/10.1177/0021998313508594>.
22. N.A. Nordendale: *Modeling and simulation of brittle armors under impact and blast effects*, Tennessee: Vanderbilt University, 2013. <https://etd.library.vanderbilt.edu/available/etd-08132013-114834/unrestricted/Nordendale.pdf>.
23. H.K. Şenyilmaz, G. Ceylan, V. Alankaya, A. Kurultay: Effect of material model to the result of high velocity impact analysis, *J. Nav. Sci. Eng.*, 10, 2014, 48–65.
24. Z. Fawaz, W. Zheng, K. Behdian: Numerical simulation of normal and oblique ballistic impact on ceramic composite armours, *Compos. Struct.*, 63, 2004, 387–395. [https://doi.org/10.1016/S0263-8223\(03\)00187-9](https://doi.org/10.1016/S0263-8223(03)00187-9).
25. O.M. Sanusi, O.A. Oyeleran, J.A. Badmus: Ballistic study of alumina ceramic-steel composite for structural applications, *J. Ceram. Process. Res.*, 21, 2020, 501–507. <https://doi.org/10.36410/jcpr.2020.21.4.501>.
26. O.M. Sanusi, M. Dauda, M. Sumaila, A.S. Ahmed, M.T. Isa, O.A. Oyeleran, O.O. Martins: Compositions Optimization of Antang Corundum for Developing Advanced Ceramic, *Aceh Int. J. Sci. Technol.*, 7, 2018, 32–43. <https://doi.org/10.13170/aijst.7.1.8770>.
27. Abaqus: *Abaqus Theory Manual and User’s Manual*, Dassault Systemes Simulia Corp., Providence, RI, USA, 2012.
28. NIJ Standard 0108.01: *Ballistic Resistant Protective Materials*, National Institute of Justice. (1985). <https://www.ncjrs.gov/pdffiles1/nij/099859.pdf>.
29. P. Kędziński, A. Morka, G. Sławiński, T. Niezgodza: Optimization of two-component armour, *Bull. Polish Acad. Sci. Tech. Sci.*, 63, 2015, 173–179. <https://doi.org/10.1515/bpasts-2015-0020>.
30. C.W. Isaac, O. Oluwole: Numerical modelling of the effect of non-propagating crack in circular thin-walled tubes under dynamic axial crushing, *Thin-Walled Struct.*, 115, 2017, 119–128. <https://doi.org/10.1016/j.tws.2017.02.012>.
31. M. Lee, Y.H. Yoo: Analysis of ceramic/metal armour systems, *Int. J. Impact Eng.*, 25, 2001, 819–829. [https://doi.org/10.1016/S0734-743X\(01\)00025-2](https://doi.org/10.1016/S0734-743X(01)00025-2).
32. C.W. Isaac: Crushing response of circular thin-walled tube with non-propagating crack subjected to dynamic oblique

- impact loading, *Int. J. Prot. Struct.*, 11, 2020, 41–68. <https://doi.org/10.1177/2041419619849087>.
33. A.P.T.M.J. Lamberts: Numerical simulation of ballistic impacts on ceramic material, Netherlands: Eindhoven University of Technology, 2007. <http://www.mate.tue.nl/mate/pdfs/8206.pdf>.
34. D. Burger, M. V Donadon, F. Cristovao, S.F. Muller: Formulation and implementation of a constitutive model for brittle materials in Abaqus explicit finite element code, in: *Proc. COBEM—20th Int. Congr. Mech. Eng.*, Gramado, Brazil, Gramado-RS: Brazilian Association of Engineering and Mechanical Sciences, p. 1–12, 2009.
35. L. Ming, O. Pantalé: An efficient and robust VUMAT implementation of elastoplastic constitutive laws in Abaqus/Explicit finite element code, *Mech. Ind.*, 19, 2018, 308. <https://doi.org/10.1051/meca/2018021>.
36. D.S. Cronin, K. Bui, C. Kaufmann, G. Mcintosh, T. Berstad: Implementation and Validation of the Johnson-Holmquist Ceramic Material Model in LS-Dyna, in: *4th Eur. LS-DYNA Users Conf.*, Germany, Ulm: DYNA, p. 47–60, 2004.
37. J. Hub, P. Kneys: 3D Simulation Analysis of Aircraft Protection Material, *University Review*, 7, 2013, 15–19.
38. L. Turhan, Ö. Eksik, E.B. Yaln, A. Demirural, T. Baykara, V. Günay: Computational simulations and ballistic verification tests for 7.62mm AP and 12.7mm AP bullet impact against ceramic metal composite armours, *WIT Trans. Built Environ.*, 98, 2008, 379–388. <https://doi.org/10.2495/SU080371>.
39. M. Hajheydari, S.A. Eftekhari: Simulation and numerical analysis of optimized ceramic-composite armor under vertical ballistic impact, *Int. J. Basic Sci. Appl. Res.*, 3, 2014, 184–199.
40. A. Healey: *Understanding the ballistic event: Methodology and observations relevant to ceramic armour*, England: University of Surrey, 2017.
41. MIL-STD-662F: *V50 Ballistic Test for Armor*, Dep. Def. Test Method Stand., 1997. http://everyspec.com/MIL-STD/MIL-STD-0500-0699/MIL-STD-662F_6718/.
42. P. Gotts: International ballistic and blast specifications and standards, in: *Lightweight Ballistic Composites*, Second, A. Bhatnagar (Ed.), Amsterdam: Woodhead Publishing, Elsevier Ltd., p. 115–156, 2016. <https://doi.org/http://dx.doi.org/10.1016/B978-0-08-100406-7.00005-2>.
43. Ş.H. Atapek: Development of a New Armor Steel and its Ballistic Performance, *Def. Sci. J.*, 63, 2013, 271–277. <https://doi.org/10.14429/dsj.63.1341>.
44. N. Kiliç, B. Ekici: Ballistic resistance of high hardness armor steels against 7.62 mm armor piercing ammunition, *Mater. Des.*, 44, 2013, 35–48. <https://doi.org/10.1016/j.matdes.2012.07.045>.
45. T. Wierzbicki: Petalling of plates under explosive and impact loading, *Int. J. Impact Eng.*, 22, 1999, 935–954. [https://doi.org/10.1016/S0734-743X\(99\)00028-7](https://doi.org/10.1016/S0734-743X(99)00028-7).
46. P.K. Jena, B. Mishra, K. Siva Kumar, T.B. Bhat: An experimental study on the ballistic impact behavior of some metallic armour materials against 7.62mm deformable projectile, *Mater. Des.*, 31, 2010, 3308–3316. <https://doi.org/10.1016/j.matdes.2010.02.005>.